SIZE EFFECT MECHANISMS IN NUMERICAL CONCRETE FRACTURE

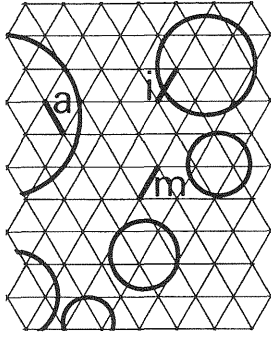J.E. Bolander Jr.
University of California, Davis, CA
Y. Kobashi
Shimizu Corporation, Tokyo, Japan

Abstract
A lattice model is used for analyzing fracture in concrete CT specimens of differing scale. Six specimens are simulated at each of three scales for comparison with experimental results. The lattice model provides estimates of fracture process zone size and the distribution of damage and energy consumption within its limits. Peripheral microcracking, though extensive, consumes very little energy relative to the mechanisms involved in actual material separation. Of particular interest is the dependence of fracture energy on both strain gradient and specimen size. Size effects witnessed in the numerical concrete agree well with experimental trends.

1 Introduction

Fracture analyses based on discretizations at the material mesoscale, as promoted by Roelfstra et al. (1985), are becoming more feasible due to advances in computing technology. In this research, the lattice model developed by Schlangen and van Mier (1992) is mod-

a : aggregate

m: matrix

i : interface

Fig. 1. Lattice model of a three-component material

ified to better represent the three-dimensional nature of concrete material and fracture processes. This lattice model is then used to analyze fracture in concrete specimens of differing scale. The analyses provide detailed descriptions of damage and energy consumption within the fracture process zone (FPZ). Variances in local fracture energy occur due to material heterogeneity and the effects of strain gradient. The latter of these causes appears to contribute to an overall size effect, that is the dependence of specific fracture energy on specimen scale.

2 Lattice modeling of concrete fracture

A lattice network of beam elements is used to model the concrete mesoscale structure, which is made of three components (Fig. 1): aggregate (a), matrix (m), and aggregate-matrix interface (i). Beam properties are assigned according to their location relative to the three components (Schlangen and van Mier, 1992). The aggregate particles are distributed so as to represent an actual material.

The effective stress acting in each element is computed as:

$$\sigma = \frac{\beta}{(1-\Omega)} \left(\frac{F}{A} + \alpha \frac{\max(|M_1|, |M_2|)}{W} \right) \tag{1}$$

where A and W are beam cross-section area and section modulus; M_1, M_2, and F are the beam end moments and axial force; α is a parameter to control the influence flexure has on fracture; and β is a parameter for scaling beam effective stress to global stress levels. The settings for α and β are discussed later in this paper. Ω is described next.

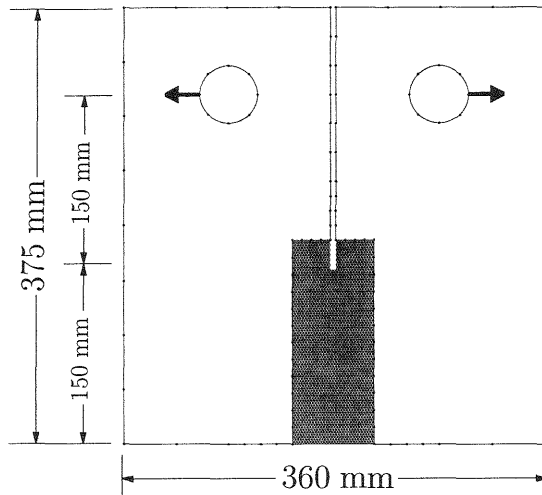For each solution cycle, the lattice element with the highest

Fig. 2. Concrete CT specimen model ($L = 150\,\mathrm{mm}$)

stress ratio $\sigma/\sigma_f \geq 1$ experiences a 'fracture event', where σ_f represents the component strength. Conventional algorithms reduce element stiffness to zero upon violation of the fracture criterion. Such models behave as if the local structure and fracture process extend uniformly through the specimen width. To better model the three-dimensional nature of the material and fracture process, the stiffness of fracturing elements is gradually reduced via damage parameter Ω, which ranges from 0 to 1 and is dependent on component type. Since local failure results in a loss of effective load carrying area, stresses increase in the yet intact material. For this reason Ω is present in Eq. 1. Additional details are given in Bolander (1995).

3 Fracture in specimens of differing scale

Concrete CT fracture specimens tested by Wittmann et al. (1990) are analyzed. Their program considered three series of specimens having ligament lengths $L = 150$, 300, and 600 mm; each series differed only in scale, except for specimen thickness which is constant.

Modeling of the $L = 150$ mm series is shown in Fig. 2. A two-dimensional lattice network composes the central region where fracture is likely to occur. Super elements constructed from plane stress boundary element equations are used to model the surrounding regions. Compatibility is maintained along the lattice region borders by constraining the displacements of the perimeter lattice nodes. Loading is applied via displacement control at the points indicated

in the figure. Weak interfacial strength is assumed for modeling normal concrete, that is $\sigma_f^a : \sigma_f^m : \sigma_f^i = 8 : 4 : 1$.

Provided the fracture process is rather localized, it is not necessary to discretize the fracture domain using the entire lattice region shown in Fig. 2. Computational demands have been greatly reduced by using an adaptive procedure which models only the FPZ and its immediate vicinity with the lattice model (Bolander, 1995). That is, the active lattice region and the boundary element constructs are updated as the FPZ travels along the ligament length.

For direct comparisons with experimental results, six specimens are analyzed at each scale. Fig. 3 shows typical results for the largest scale specimens ($L = 600$ mm). Smaller scale specimens provide similar results (Bolander, 1995). Fig. 3a shows the distribution of energy consumed over the entire loading history. The same results are presented in Fig. 4 for fracture up through about 150 mm of the ligament length. These contours are plotted using a log scale (i.e. consecutive contour energies differ by a factor of ten) with darker levels indicating higher energies. 97 to 99+% of the fracture energy is consumed by processes leading to discrete crack formation; peripheral 'microcracking' consumes a very small fraction of the total fracture energy. These results are supported by analytical work of Nirmalendran and Horii (1992).

Fig. 3b illustrates the distribution of damage over the lattice region. Lattice elements which are completely damaged, i.e. $\Omega = 1$, have been removed from the mesh. Those suffering partial damage are plotted using thinner lines. The fracture process widens out from the notch tip, reaches a maximum width over the central portion of the ligament, and then narrows under the influences of higher strain gradient and confinement when approaching the compression face of the specimen. Highly damaged elements occur within a width of roughly $1d_a$ or less, agreeing with experimental observations of Du et al. (1990) and van Mier (1991).

Fluctuations in local fracture energy, g_f, along the ligament length are related to material heterogeneity (Fig. 3c). The lower energies often correspond to locations where the main crack follows an interfacial region. Higher energies generally correspond to locations where fracture advances through the matrix, the greatest peaks occurring where failure involves a bridging mechanism. Introducing a variable damage measure (i.e. Ω) helps temper the variance in local fracture energy.

Averaging the g_f values provided by the six specimens within each series makes it easier to recognize general trends (Fig. 5). $\overline{g}_f$ increases with distance from the notch tip, then is rather constant
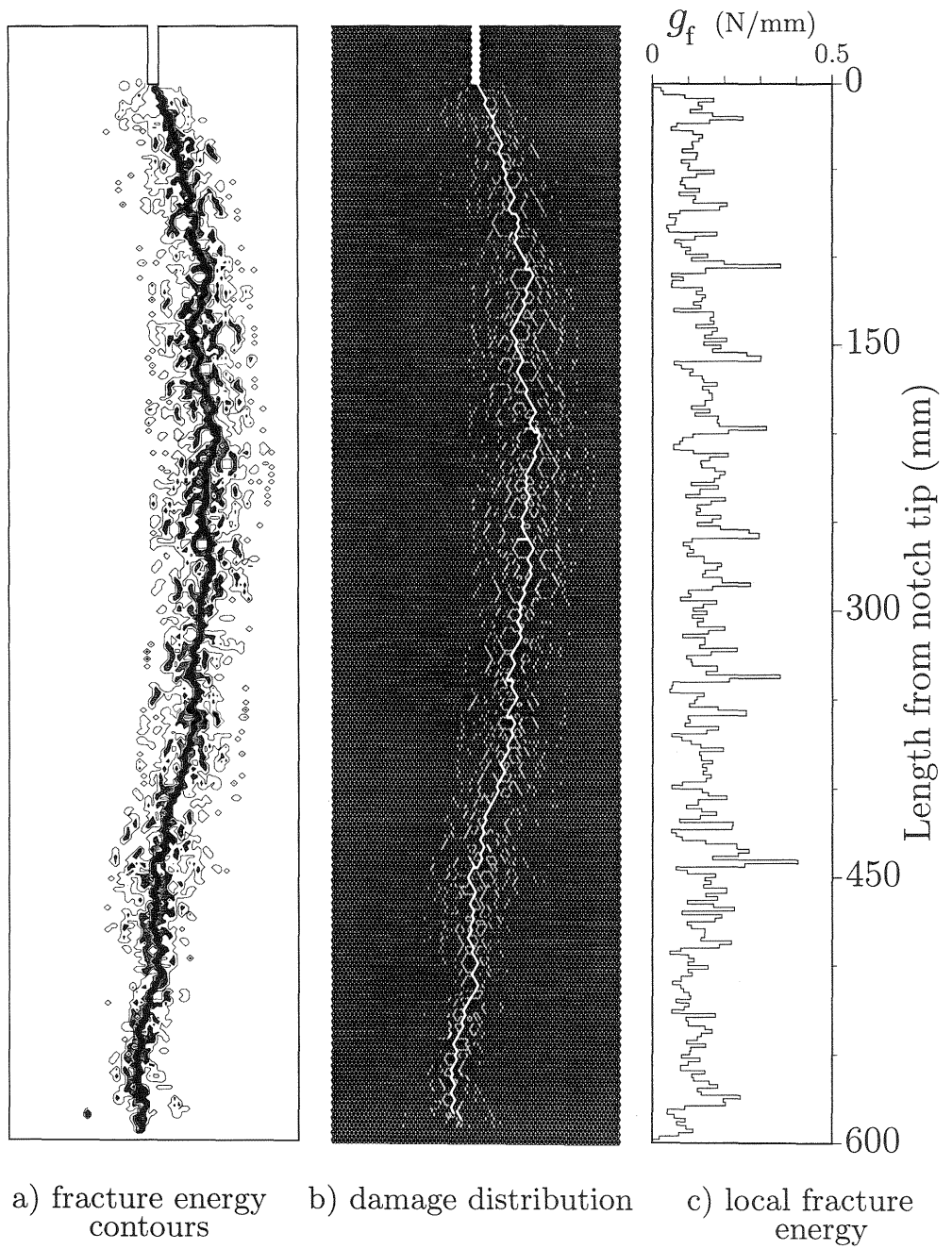
a) fracture energy   b) damage distribution   c) local fracture
   contours   energy

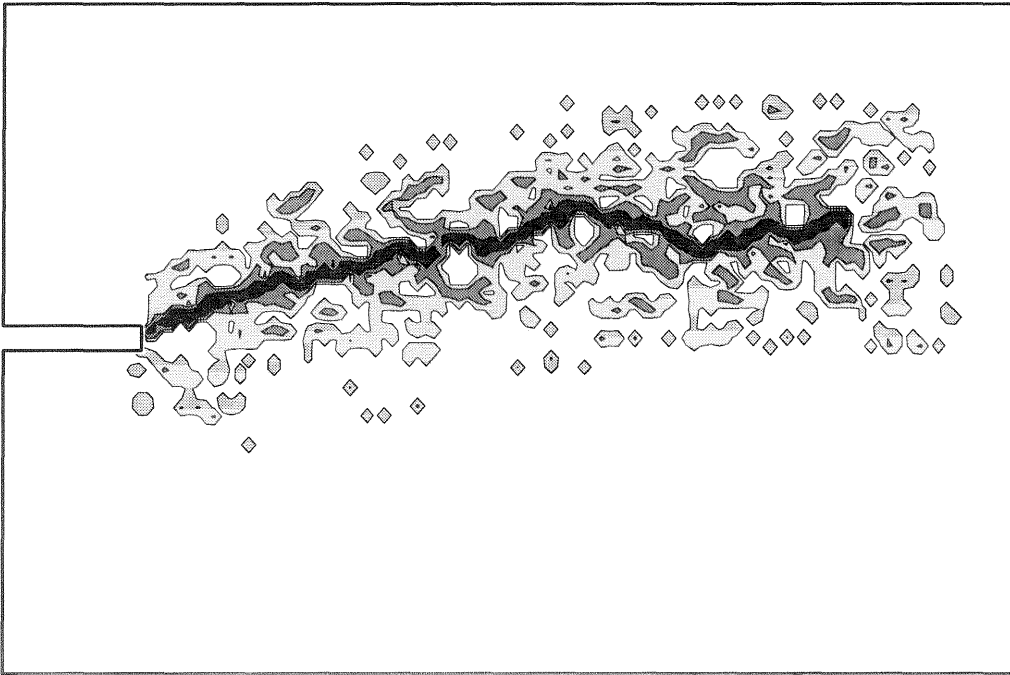Fig. 3. Typical fracture response ($L = 600\,\mathrm{mm}$)

Fig. 4. Fracture energy contours (through intermediate load stage)

over the central portion of the ligament, and eventually becomes smaller when nearing the compression face of the specimen. The average global specific fracture energy, G_f, computed for each series is also indicated in each plot.

Fig. 6 compares the numerical results with experimental scatter. The symbols indicate mean values and the error bars indicate standard deviations. It should be mentioned that previous results and those in Fig. 6a were obtained using $\alpha = 0.1$ and $\beta = 0.2$. Since the lattice model provides an overly brittle post-peak response, it is difficult to match both specific fracture energy and peak loads with a single parameter setting. For comparing with experimental peak loads, $\beta = 0.3$ was used. Our main interest is to show that various size effects are produced by models based on discretizations of the material structure. Furthermore, given the limitations of two-dimensional lattice models, strict determinations of these parameters are not justified.

The numerical concrete exhibits size effects similar to those seen experimentally. However, there are some interesting differences. For the experimental series, mean values for G_f have leveled off by ligament lengths $L = 300\,\text{mm}$. The numerical series shows a decrease
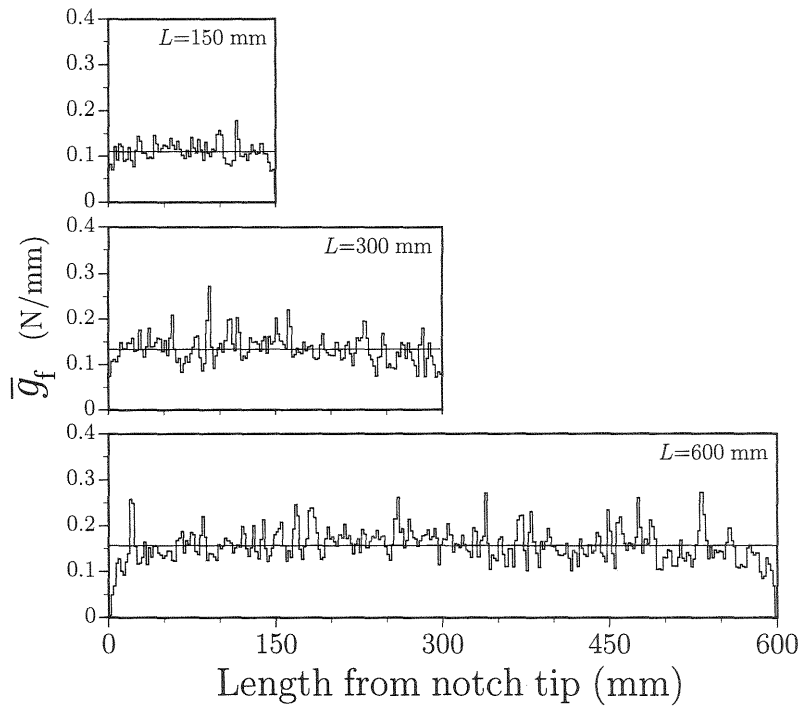
Fig. 5. Local fracture energy variance along ligament length
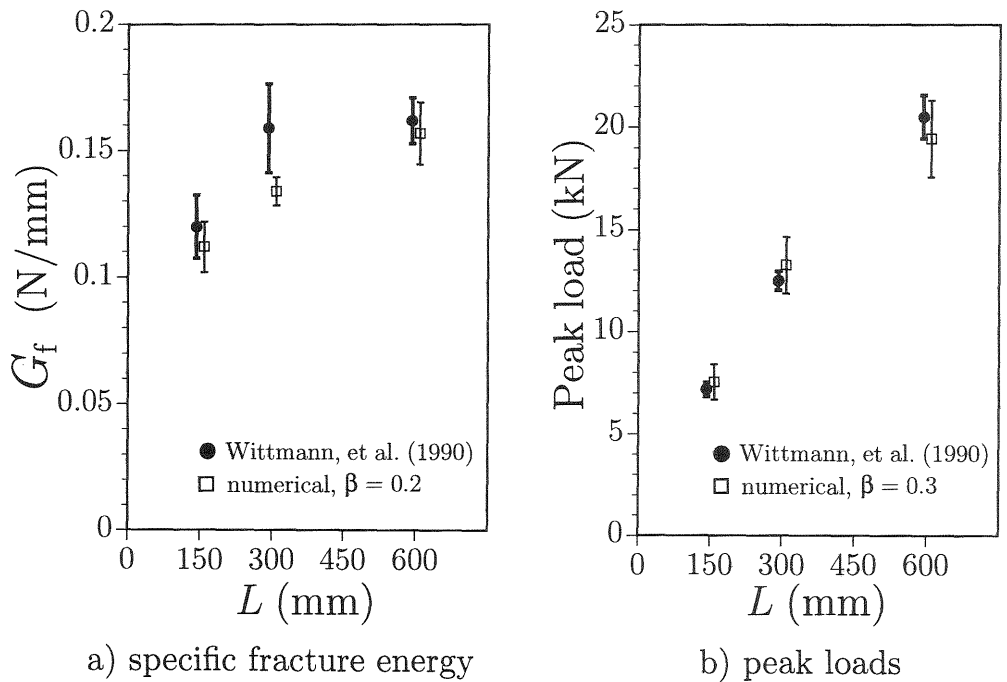

a) specific fracture energy

b) peak loads

Fig. 6. Comparing global response quantities

in the rate at which G_f increases with L, yet it is not clear if G_f becomes constant before $L = 600\,\text{mm}$. Peak loads agree remarkably well, although variance is much greater for the numerical series.

4 Conclusions

A lattice model was developed and applied to simulating fracture in concrete CT specimens of differing scale. Several conclusions can be made:

1. Fluctuations in local fracture energy are related to material heterogeneity. When averaged over several specimens, local fracture energy increases with distance from the notch tip, becomes essentially constant over the ligament midlength, and then decreases when nearing the compressive face of the specimen.
2. About 97 to 99+% of the total fracture energy is consumed in a width of $1d_a$ centered about the macrocrack; peripheral microcracking consumes relatively little energy.
3. The numerical concrete exhibits size effects which agree well with experimental trends.
4. Random material modelings allow for comparisons with series of test specimens, not only in the mean value sense but also with respect to variances of the response quantities. This quality is important in researching material behavior.

5 References

Bolander, J.E. (1995) Mesoscopic analyses of fracture in cement-based composites. Univ. of California, Davis, Dept. Civil & Envir. Engng. Report (in preparation)

Du, J.J., Kobayashi, A.S. & Hawkins, N.M. (1990) An experimental-numerical analysis of fracture process zone in concrete fracture specimens. **Engng. Fracture Mech.**, 35(1/2/3), 15-27.

van Mier, J.G.M. (1991) Mode I fracture of concrete: Discontinuous crack growth and crack interface grain bridging. **Cem. and Conc. Res.**, 21, 1-15.

Nirmalendran, S. & Horii, H. (1992) Analytical modelling of microcracking and bridging in fracture of quasi-brittle materials. **J. Mech. Phys. Solids**, 40 (2), 863-886.

Roelfstra, P.E., Sadouki, H., & Wittmann, F.H. (1985) Le béton numérique. **Mat. et Constr.**, 107, 327-335.

Schlangen, E. & van Mier, J.G.M. (1992) Experimental and numerical analysis of micromechanisms of fracture of cement-based composites. **Cem. & Conc. Composites**, 14, 105-118.

Wittmann, F.H., Mihashi, H. & Nomura, N. (1990) Size effect on fracture energy of concrete. **Engrg. Fracture Mech.**, 35(1/2/3), 107-115.